Correlated errors in GPS position time series: Implications for velocity estimates

Alvaro Santamaria-Gomez, Marie-Noëlle Bouin, Xavier Collilieux, Guy Woppelmann

Correlated errors in GPS position time series: Implications for velocity estimates

Alvaro Santamaría-Gómez,[1,2] Marie-Noëlle Bouin,[3] Xavier Collilieux,[2] and Guy Wöppelmann[4,5]

Received 15 May 2010; revised 30 September 2010; accepted 21 October 2010; published 20 January 2011.

[1] This study focuses on the effects of time correlation in weekly GPS position time series on velocity estimates. Time series 2.5 to 13 years long from a homogeneously reprocessed solution of 275 globally distributed stations are analyzed in terms of noise content and velocity uncertainty assessment. Several noise models were tested, including power law and Gauss-Markov processes. The best noise model describing our global data set was a combination of variable white noise and power law noise models with mean amplitudes of ~2 mm and ~6 mm, respectively, for the sites considered. This noise model provided a mean vertical velocity uncertainty of ~0.3 mm/yr, 4–5 times larger than the uncorrelated data assumption. We demonstrated that correlated noise content with homogeneously reprocessed data is dependent on time series length and, especially, on data time period. Time series of 2–3 years of the oldest data contain noise amplitude similar to that found for time series of 12 years. The data time period should be taken into account when estimating correlated noise content, when comparing different noise estimations, or when applying an external noise estimation to assess velocity uncertainty. We showed that the data period dependency cannot be explained by the increasing tracking network or the ambiguity fixation rate but is probably related to the amount and quality of recorded data.

Citation: Santamaría-Gómez, A., M.-N. Bouin, X. Collilieux, and G. Wöppelmann (2011), Correlated errors in GPS position time series: Implications for velocity estimates, *J. Geophys. Res.*, *116*, B01405, doi:10.1029/2010JB007701.

1. Introduction

[2] To investigate geophysical phenomena, secular velocities of discrete points on the Earth's surface are commonly estimated today from position time series of permanent GPS stations. Horizontal velocities have been used for decades to derive global plate kinematics [e.g., *Argus and Heflin*, 1995; *Larson et al.*, 1997; *Kogan and Steblov*, 2008] or to study regional tectonics [e.g., *McClusky et al.*, 2000; *Marquez-Azua and DeMets*, 2009]. More recently, GPS vertical velocities have been used to study subduction zones [e.g., *Bergeot et al.*, 2009], to assess postglacial rebound processes [e.g., *Nocquet et al.*, 2005; *Sella et al.*, 2007] or to correct long-term sea level records from tide gauges [e.g., *Wöppelmann et al.*, 2009]. For all these applications, unbiased velocities and realistic uncertainty estimates are mandatory. However, several issues are known to affect velocity estimation, for instance reference frame errors [*Argus et al.*, 1999], seasonal signals [*Blewitt and Lavallée*, 2002], position offsets [*Williams*, 2003a], and antenna phase center model errors [*Cardellach et al.*, 2007; *Steigenberger et al.*, 2009a]. In general, all nonmodeled physical phenomena or neglected correlated noise content generate processes that affect velocity uncertainty estimation [e.g., *Williams et al.*, 2003b]. Noise sources result from mismodeling of orbits [*Griffiths and Ray*, 2009; *Steigenberger et al.*, 2009b], atmospheric effects (loading and tropospheric delay) [e.g., *Tregoning and Watson*, 2009], correlation through estimated parameters within the GPS data processing, and station-dependent effects like monument instability [*King and Williams*, 2009] or near-field multipath [e.g., *King and Watson*, 2010; F. Dilssner et al., Impact of near-field effects on the GNSS position solution, paper presented at 21st International Technical Meeting of the Satellite Division of the Institute of Navigation, Savannah, Ga., 2008]. To properly infer valuable geophysical information, the noise effects on velocity estimates need to be taken into account.

[3] When rates are estimated without any a priori data covariance information, the noise content is usually assumed to be uncorrelated, thus simplifying the covariance matrix into a diagonal matrix. Assuming that the sampling rate

[1]Instituto Geográfico Nacional, Yebes, Spain.
[2]Institut Géographique National, Marne-la-Vallée, France.
[3]Centre National de Recherches Météorologiques, Météo France, Brest, France.
[4]Littoral Environnement et Sociétés, Université de La Rochelle, CNRS, La Rochelle, France.
[5]Fédération de Recherche en Environnement pour le Développement Durable, La Rochelle, France.

0148-0227/11/2010JB007701

(ΔT) is constant (equally spaced data) and that the number of points (N) is large, then the trend variance is approximated by [*Zhang et al.*, 1997; *Williams*, 2003b; *Bos et al.*, 2008]:

$$\sigma_r^2 \approx \frac{12 \cdot a^2}{N \cdot T^2} = \frac{12 \cdot a^2}{\Delta T^2 \cdot (N^3 - N)}, \quad (1)$$

where a represents the uncorrelated (white) noise amplitude and T is the time series length. Formal trend uncertainties are then proportional to the uncorrelated noise amplitude and inversely proportional to the number of points and the time series length. This way, by incrementing the sampling interval or the observation time span, the trend uncertainty is considerably reduced. Estimated formal velocity uncertainties may be very small. Some studies estimating rates assuming uncorrelated data reevaluated the estimated rate uncertainties from χ^2 adjustments [e.g., *Khan et al.*, 2008], or equivalently, from a posteriori variance scaling factors [e.g., *Calais et al.*, 2006; *Argus and Peltier*, 2010].

[4] Early studies detected time-correlated noise in several geodetic data sets including GPS data [*Wyatt*, 1982, 1989; *Langbein and Johnson*, 1997; *Zhang et al.*, 1997]. Owing to this unaccounted time-correlated noise, rate uncertainties were estimated to be too optimistic up to one order of magnitude [*Zhang et al.*, 1997; *Mao et al.*, 1999]. This way, assuming that the covariance matrix reflects time-dependent positions, for example by supposing that station monuments move following a random walk process, then the formal uncertainty of the estimated velocities is approximated by [*Zhang et al.*, 1997; *Williams*, 2003b; *Bos et al.*, 2008]:

$$\sigma_r^2 \approx \frac{b^2}{T} = \frac{b^2}{\Delta T \cdot (N - 1)}, \quad (2)$$

where b represents the random walk noise amplitude. Equation (2) shows that in the presence of heavily correlated time series, velocity uncertainties are significantly augmented with respect to those from uncorrelated time series. In this case, the addition of more (correlated) positions by extending the observation span barely reduces the formal rate uncertainty. Moreover, changing the sampling interval, while keeping the observation span constant, does not affect the estimated formal uncertainties at all.

[5] The study of noise processes in GPS position time series has been conducted on station position time series from regional and global networks. Regional solutions filter out some level of common correlated noise content, constituting then interesting data sets to investigate specific local noise sources as monument noise [e.g., *Zhang et al.*, 1997; *Beavan*, 2005; *Williams et al.*, 2004; *Langbein*, 2008]. Conversely, noise analyses of global solutions are appropriate to investigate technique-related noise sources such as reference frame and orbit, troposphere or loading mismodeling [e.g., *Mao et al.*, 1999; *Williams et al.*, 2004; *Amiri-Simkooei et al.*, 2007]. For all these global noise analyses with nonreprocessed data, a combination of white and flicker noise is commonly used to describe the stochastic properties of the position time series. Most of these authors used the Maximum Likelihood Estimation (MLE) technique.

[6] Here we analyze the noise content of a global reprocessed vertical velocity field formed by 275 stations spanning up to 13 years (section 2). We investigate if noise properties found in past global analyses are still relevant to longer reprocessed time series and whether they can be assumed to be constant with time. If we cannot assume this, can we derive a time-dependent general rule to account for the noise content impact on velocity uncertainties? We focused on the vertical component only because it is the most susceptible to noise. However, results obtained on the vertical component are largely transposable to the horizontal components. Before the noise analysis, existing periodic signals in time series were analyzed and removed in a station-by-station basis (section 3). A wide range of noise models were analyzed to give the general noise content of a reprocessed global GPS solution and, more specifically, a reevaluation of the vertical rate uncertainty for each station of the velocity field (section 4). The long time series used here allowed us to infer time-dependent colored noise properties and thus to investigate how and why time-correlated GPS noise content varies with time (section 5).

2. Data

[7] Several global vertical velocity field solutions with different station networks, time spans, and processing strategies have been released throughout time by the University of La Rochelle Analysis Center Consortium (ULR) since its creation in 2002 [*Wöppelmann et al.*, 2004, 2007, 2009]. In this paper, we analyze the fourth ULR solution (ULR4 hereafter). This solution is based on a homogeneous reprocessing of a global network of 316 stations from January 1996 to December 2008 using the GAMIT/GLOBK package [*Herring et al.*, 2008]. We applied up-to-date models and procedures following the International Earth Rotation Service (IERS) standards [*McCarthy and Petit*, 2004] and the International GNSS Service (IGS) [*Dow et al.*, 2009] recommendations (http://acc.igs.org/reprocess.html). For instance, we used the absolute antenna phase calibration model [*Schmid et al.*, 2007], cutoff angle of 10°, phase cycle ambiguity fixation, VMF1 grids [*Boehm et al.*, 2006; *Kouba*, 2007] for tropospheric delay, FES2004 model [*Lyard et al.*, 2006] for ocean tide loading, and no higher ionospheric effects or atmospheric loading were corrected for. We processed the GPS data estimating daily station positions, satellite orbits, and Earth orientation parameters. To optimize the data processing, the station network was split in several subnetworks. A dedicated station distribution scheme using daily optimized subnetworks was devised to improve the network geometry. Subnetwork loose solutions were combined into daily and then into weekly solutions using the combination model described by *Dong et al.* [1998]. The resulting 678 weekly solutions were provided to the IGS TIGA pilot project [*Schöne et al.*, 2009] and to the first IGS reanalysis campaign (http://acc.igs.org/reprocess.html). More details about the GPS data processing strategy implemented for the ULR4 solution are given by *Santamaría-Gómez et al.* [2011] and are not repeated here.

[8] Station velocities were estimated combining these 678 weekly solutions into a long-term solution using CATREF software [*Altamimi et al.*, 2007]. Seasonal signals (annual and semiannual) were removed before velocity estimation.

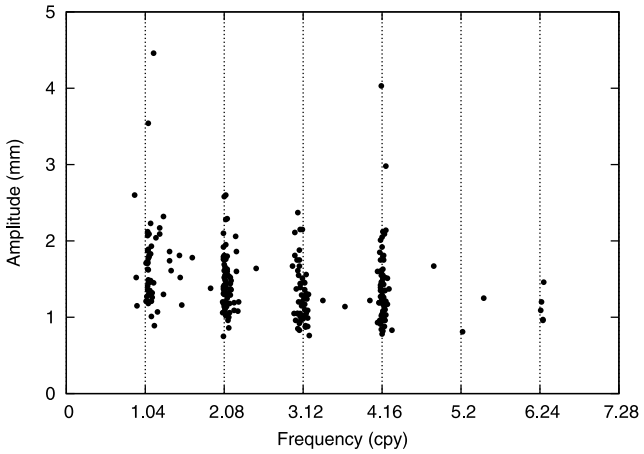

Figure 1. Significant periodic signals using a frequency-dependent SNR threshold. Only the first seven harmonics of the 1.04 cpy frequency are shown.

From the resulting residual position time series, only those having a minimum length of 2.5 years were retained in the velocity field, thus avoiding biased velocities due to unreliable estimated seasonal signals [*Blewitt and Lavallée*, 2002] and underestimated velocity uncertainties due to absorbed correlated noise content in estimated trends of short time series [*Williams et al.*, 2004; *Bos et al.*, 2010]. This led to 275 residual position time series with lengths between 2.5 and 13 years. Each of these residual time series was used in the noise analysis described in section 4 to address station velocity uncertainties. Although seasonal signals were already removed, remaining periodicities were analyzed and removed before the noise analysis, as described in section 3.

3. Periodic Signals Analysis

[9] Residual position time series may be represented by a sum of parameters of interest and background noise. Thus data that is not described by the functional model (represented here by station rates and significant periodic signals) will be captured by the stochastic model. Noise parameters are sensitive to superimposed signals present in time series [*Mao et al.*, 1999; *Beavan*, 2005; *Williams and Willis*, 2006; *Amiri-Simkooei et al.*, 2007]. For instance, neglecting seasonal signals could produce power law estimates biased to higher values [*Blewitt and Lavallée*, 2002]. To avoid biased estimates of correlated noise content, any significant periodic signal must be removed from the time series. Seasonal signals were already removed prior to velocity estimation (section 2). We nevertheless verified the presence of remaining periodicities using a nonlinear iterative least squares method to detect the most powerful spectral lines [*Mignard*, 2005; *Collilieux et al.*, 2007]. Median spectral resolution is 0.1 cpy, equivalent to a median time series length of 10 years. Only significant signals with frequency higher than the annual frequency were retained. Signal significance is based on the signal-to-noise ratio (SNR), which is the ratio between the spectral line amplitude and the median spectrum. That is, SNR is dependent on the assumed background noise. Thus, using a white background noise, low-frequency signals may be flagged as significant, whereas we want to interpret them as being background noise. The rigorous approach to estimate the significance of detected frequency signals is to use a background noise as realistic as possible, for instance, a flicker noise model in global GPS position time series. Here, we devised a simpler approach based on a frequency-dependent decay SNR threshold to assign the significance of detected signals. Using a white background noise and a SNR threshold of 4, the SNR of all detected signals was extracted. A nonlinear regression equation ($y = ax^b$) was fitted to be used as SNR threshold. This approach yielded a frequency-dependent SNR threshold between 4 for the highest frequencies and 6 for near-annual frequencies.

[10] The resulting significant signals (Figure 1) were centered nearby the harmonics of the GPS "draconitic" year period (approximately 351.2 days or 1.04 cpy), i.e., the revolution period of the GPS constellation in inertial space with respect to the Sun, in agreement with *Ray et al.* [2008]. Very little significant amplitudes were found from the fourth harmonic onward. The mapping of these draconitic harmonics into position time series may be driven by orbit mismodeling, atmospheric loading, or station-dependent multipath errors [*Ray et al.*, 2008; *Tregoning and Watson*, 2009; *King and Watson*, 2010]. It is worth noting that some significant signals were also found at the highest frequencies (~24.76 cpy or a period of ~14.75 days, not shown in Figure 1). These signals are likely due to the propagation of mismodeled tidal periods [e.g., *Penna et al.*, 2007].

[11] It is also appreciable in Figure 1 that even after removing the seasonal signals (annual and semiannual) there is still noticeable power near these bands. Some authors have already shown this effect [*Amiri-Simkooei et al.*, 2007; *Ray et al.*, 2008]. This remaining near-seasonal power could result from neglecting seasonal signals with time-varying amplitudes [*Bennett*, 2008] or harmonics of the draconitic period, but the spectral resolution is too large to really conclude on this point. The mean amplitude of the remaining signals (see Table 1) was small enough to not

Table 1. Mean Frequency and Scatter and Mean and Maximum Amplitudes of the Significant GPS Draconitic Harmonics Detected in Residual Time Series of ULR4 Solution

Draconitic Harmonic	Mean Frequency (cpy)	Scatter Frequency (cpy)	Mean Amplitude (mm)	Maximum Amplitude (mm)
1	1.09	0.10	1.7	4.5
2	2.10	0.05	1.5	2.6
3	3.10	0.07	1.3	2.4
4	4.17	0.04	1.4	4.0
6	6.27	0.02	1.1	1.5

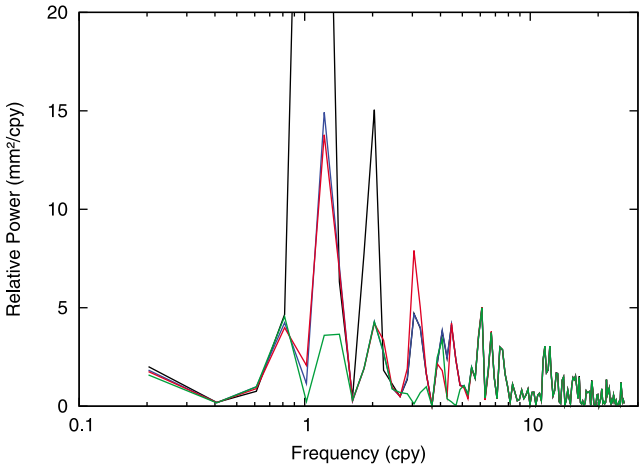

Figure 2. Vertical power spectrum for NRIL station with raw time series (black), time series without seasonal signals (blue), without seasonal plus fixed harmonics (red), and without seasonal plus station-specific signals (green). The *x* axis is in logarithmic scale.

significantly affect velocity estimation. The maximum values of these harmonics reach 4 mm at KODK station close to the annual period and at ALRT station in the fourth harmonic. For the ALRT station, this signal does not affect the velocity estimation due to its high frequency. For KODK, this signal corresponds to a bias of 0.2 mm/yr in the velocity estimation if suitable parameters are not estimated. Therefore the impact of these harmonics on velocity estimates can be neglected for most applications.

[12] Figure 1 and Table 1 also show that the estimated frequencies for the first three harmonics are a little scattered, especially the first one. In addition, there are some significant signals that are apparently not related to these harmonics. These signals might result from real loading effects, from tidal EOP mismodeling [*Gross*, 2009] or from the propagation of unmodeled or mismodeled periodic loading, which could be station-dependent since they are functions of the relative position of stations and satellites [*Stewart et al.*, 2005; *Penna et al.*, 2007; *Tregoning and Watson*, 2009]. Another station-dependent effect is multipath, which might be one of the causes of the mapping of the orbit draconitic periods into position time series [*King and Watson*, 2010]. In addition, the draconitic period varies for each satellite and over time [*Choi et al.*, 2004; *King and Watson*, 2010], so its effect on position time series might not be purely harmonic. In this sense, note that annual draconitic frequencies of Figure 1 might be slightly biased high, although the mean value (see Table 1) lies within the mean frequency resolution (0.1 cpy).

[13] In our study, to avoid a biased noise analysis, instead of removing a mean frequency for these signals, the detected significant signals (up to 10 per station from near-annual to the Nyquist frequency) were removed on a station-by-station basis, following *Amiri-Simkooei et al.* [2007]. With this procedure, all station-dependent significant peaks from near-annual to the highest frequencies were properly filtered out while preserving the background noise to be estimated with MLE. For instance, Figure 2 shows four power spectra estimated using the Lomb-Scargle periodogram [*Press et al.*, 1992] for the NRIL station corresponding to the raw time series (no periods removed) and to the time series with different periodic signals removed (seasonal, seasonal plus fixed draconitic, and seasonal plus station-specific). The raw spectra (solid black line in Figure 2) contained all the periodicities, notably a prominent annual signal. When seasonal signals were removed (dotted blue line in Figure 2), the remaining peaks corresponded mainly to the draconitic periods already shown in Figure 1. However, by removing these fixed draconitic periods (dashed red line in Figure 2), there was remaining and significant power near 1 and 3 cpy frequencies. When removing station-specific harmonic terms, these signals were also filtered out (solid green line in Figure 2). The effect of remaining peaks (e.g., fourth and sixth harmonic) was estimated to be insignificant on the noise analysis of section 4.

4. Noise Analysis

4.1. Noise Models

[14] Noise models tested here were formed by combining white and colored noise components. White noise components tested were constant white noise (WH) amplitude, variable white noise amplitude (VW), and time-dependent white noise (TW) amplitude. The WH model has a constant variance. The VW model uses the formal errors of the residual time series and solves for a variance scale parameter. The TW model, in addition to the constant term of the WH model, fits an exponential decay term, which represents time-dependent amplitude of the white noise over a finite time span [*Williams and Willis*, 2006]. Colored noise components tested were power law and Gauss-Markov processes. The power law process [*Agnew*, 1992] follows a power spectrum of

$$P_x(f) = P_0 \cdot f^k, \tag{3}$$

where P_0 is a normalizing constant, f is temporal frequency, and k is the spectral index defining the frequency dependence of the process. Specific power law models with integer spectral index are named flicker noise (FN) for $k = -1$ and random walk (RW) for $k = -2$. When k is to be estimated, this noise model was termed here as general power law (PL). The Gauss-Markov process follows a power spectrum of (S. D. P. Williams, personal communication, 2010)

$$P_x(f) = P_0(\beta^2 + 4\pi^2 f^2)^{\frac{k}{2}}, \tag{4}$$

where β is the crossover frequency representing the point where the spectrum of low and high frequencies cross each other. For lower frequencies, this process is frequency-independent (flat spectrum or $k = 0$) and for the higher frequencies, the process is consistent with a power law process. When k is to be estimated, this noise model was termed here as general Gauss-Markov (GG). The first-order Gauss-Markov (GM) noise model is a special case where $k = -2$.

Table 2. ML Ratio (δML) at 95th Percentile and Difference of Degrees of Freedom Between Different Noise Models Tested With Synthetic Data for Subsequent Model Significance Assessment

	Degree of Freedom Difference	95% δML
PL versus FN/RW	1	2.2
GM versus RW	1	4.3
GG versus FN/RW	2	5.2
GM versus PL	0	3.4
GG versus PL	1	4.0
GG versus GM	1	2.3

4.2. Optimal Noise Model Criteria

[15] We used MLE as implemented by *Williams* [2008] to address the nature and the amount of time-correlated noise in the 275 residual vertical time series (section 2). This technique has been shown to perform better than the classical spectral analysis, improving the sensitivity to the time-correlated noise content [*Langbein and Johnson*, 1997; *Mao et al.*, 1999]. Moreover, when the number of points is much larger than the number of parameters of the regression, it performs similarly to the Least Squares Variance Component Estimation [*Amiri-Simkooei et al.*, 2007].

[16] The likelihood value obtained from the MLE analysis indicates the degree of coherence between input data and an a priori chosen noise model. In order to select the best noise model to describe the data, we first analyzed the maximum likelihood ratio (δML) between different noise models. Several authors have discussed the appropriateness of the δML metric to assess model significance [*Langbein and Johnson*, 1997; *Mao et al.*, 1999; *Williams et al.*, 2004; *Langbein*, 2004, 2008; *Beavan*, 2005; *Williams and Willis*, 2006]. The δML between two different stochastic models can be used as a decision parameter if the difference in the number of estimated parameters (degrees of freedom) for each model is taken into account. Thus the simplest noise model showing a significant higher ML value is signaled as the best model to describe the data. *Williams and Willis* [2006] suggested a δML (at 95th percentile) between 2.9 and 3.1 for one degree of freedom difference and 4.7 for two degrees of freedom difference. *Langbein* [2004] proposed a value of δML (at 95th percentile) equal to 2.6 per degree of freedom difference.

[17] To obtain a proper δML threshold value specific for the noise models tested here, we used equations 7 to 9 of *Williams* [2003b] to create 1000 synthetic time series of 10 years of data (average span of ULR4 solution time series). We created 500 of them following a FN with unit noise amplitude (1 mm $yr^{-1/4}$). The other 500 were created following a RW with unit noise amplitude (1 mm yr^{-2}). The noise properties of these synthetic time series were then estimated with MLE assuming FN, PL, GM, and GG noise models. The ML values of each time series and noise model were compared. Gauss-Markov processes (GM and GG models) obtained a higher ML value for 76% of the synthetic time series, in agreement with *Langbein* [2004]. The ML value was then compared between pairs of noise models and the δML values at the 95th percentile were extracted (Table 2). If the δML between two models are larger than the correspondent value in Table 2, then the first model (left) is preferred over the second one (right). We found subtle differences in the δML values between different processes even with the same difference of degrees of freedom. It is worth noting that between the PL and GM noise models there is no difference in degrees of freedom. However, between these two models, MLE results often pointed to a GM model even though synthetic noise was a PL process (FN or RW), and also with longer synthetic time series. The 95th percentile values of Table 2 were used as a threshold to assess specific noise model significance in section 4.3.

4.3. Noise Analysis Results

[18] To provide a more realistic velocity uncertainty for the ULR4 vertical velocity field, the vertical velocity uncertainties were reestimated in a station-by-station basis using a full a priori variance-covariance matrix. To obtain the most adequate variance-covariance matrix, several noise models were tested to describe the noise content of the 275 vertical residual time series. By combining several white noise and colored noise model components, we considered 27 different stochastic models. This range of stochastic models is larger than that used in recent noise analyses of global GPS solutions [*Williams et al.*, 2004; *Amiri-Simkooei et al.*, 2007; *Wöppelmann et al.*, 2009].

[19] As described in section 4.2, the δML value between different noise models was used to identify the best noise model to describe noise content in our data. Table 3 contains the median δML value of each model, distributed by noise component, with respect to the RW model, which is the model that provides the smallest ML value.

[20] By examining results of Table 3, we can draw the following general conclusions.

4.3.1. Regarding the White Noise Models

[21] 1. Any combination of colored noise with VW was significantly superior to the other types of white noise combinations tested. When using a WH model, the MLE algorithm often found zero white noise amplitude, in agreement with the findings of *Beavan* [2005]. Conversely, with VW model there was always some level of (scaled) white noise amplitude. However, these differences between WH and VW models did not translate into significant differences in the estimated velocity uncertainties.

[22] 2. The TW model performed slightly better than the simpler WH model. But, in general, there is no appreciable exponential time-dependent decay of white noise in GPS data. Indeed, only for 2–3% of the time series, a TW was significantly detected (see supplementary material).[1] Time-variable white noise is, however, significant through the preferred VW model.

4.3.2. Regarding the Colored Noise Models

[23] 1. The mean value of the PL model was significantly larger than the other colored noise models. This may be due to an important loss of solutions for the TW+GG model, where only 86% of the time series were successfully solved (for the other models it was between 98% and 100%). These numerical issues were probably due to the large number of parameters to solve (5) for the TW+GG model and the shortness of some time series;

[24] 2. With respect to noise models with integer spectral index (FN, RW, FN+RW and GM), the FN model was

[1] Auxiliary materials are available in the HTML. doi:10.1029/2010JB007701.

Table 3. ML Ratio of Each Stochastic Model With Respect to RW Model[a]

		FN	RW	FN+RW	PL	GM	GG	
		72.4	0	72.4	93.5	89.2	93.6	
WH	41.3	93.4	82.3	60.7	93.8	93.8	93.6	79.9
VW	58.5	**116.0**	96.7	95.7	**116.1**	**113.4**	**117.0**	101.9
TW	44.8	97.6	82.4	97.6	103.3	106.1	62.0	84.8
		94.9	65.4	81.6	101.7	100.6	91.6	

[a]Stochastic models are grouped by type (white or colored). Rightmost column and bottom row represent the mean value of each noise component. The best models are shown in bold.

clearly superior to the RW model. Thus RW noise, found with different geodetic measurements and related to monument instability, was not clearly found in our results, in agreement to other global GPS solutions [*Williams et al.*, 2004]. For these global solutions, this could be due to the shortness of the time series or to the dominance of the other noise types, such as FN, which could mask the RW noise. This was also corroborated by the performance of the FN +RW model, in agreement with *Langbein*'s [2008] findings. For the time series with an estimated spectral index between -1 and −2, the δML value between PL and FN+RW is not significant. Assuming that RW is station-dependent and FN is regionally correlated [*Williams et al.*, 2004], this would indicate that, although RW may exist, it is masked under FN and it only would appear when FN is taken into account through regional noise filtering or using a FN+RW noise model. In this sense, several studies using very short baselines [e.g., *King and Williams*, 2009; *Hill et al.*, 2009] place a bound of 0.2–0.8 mm/yr$^{1/2}$ for the RW standard deviation due to monuments. Finally, GM and FN models performed similarly, due to that GM tends to mimic FN noise for the middle frequencies near the crossover period [*Langbein*, 2008].

[25] We aim at providing a noise process model that most often describes the autocorrelation of GPS height time series to be used to reevaluate velocity uncertainties estimates. We are however aware that there are station-by-station differences with such a general model (see the end of this section). This way, we will also discuss the impact using one model or another on the velocity uncertainties. From Table 3, we can exclude all models except VW+GG, VW +PL, VW+GM, and VW+FN. The δML threshold values of Table 2 are larger than the δML values found between the best four models of Table 3. This means that, regarding the δML metric, the FN, PL, GM, and GG noise models are interchangeable and no decision can be taken to select the best noise model. A different criterion must then be used to select the noise model. Thus if velocity uncertainties between these four retained models were similar there would be no issue to arbitrarily select one of them. Figure 3 represents the velocity uncertainties of the ULR4 solution estimated using the four models with the highest mean likelihood value. Vertical velocity uncertainties of VW+FN, VW+GM and VW+GG models were plotted against the VW +PL model. From Figure 3, it was clear that both GM and GG models showed more optimistic vertical velocity uncertainties than the PL model. Estimated vertical velocities were compared to vertical velocities from the recently released ITRF2008 [*Altamimi et al.*, 2010] using a 14-parameter similarity [*Altamimi et al.*, 2002]. The vertical velocity weighted RMS of the transformation is 0.5 mm/yr. On the basis of this vertical velocity discrepancy, the mean uncertainty values provided by the GG and GM models (0.19 and 0.15 mm/yr, respectively) appear to be unrealistically small. These models also provide optimistic rate

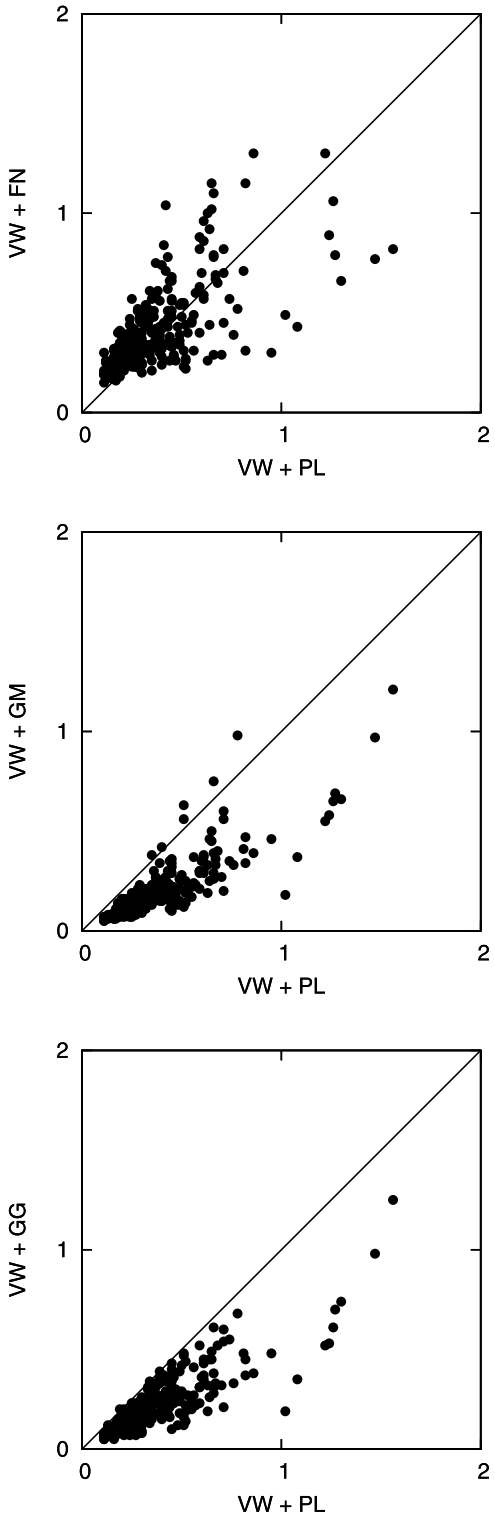

Figure 3. Comparison of vertical velocity uncertainties (in mm/yr) between VW+PL model and (top) VW+FN, (middle) VW+GM, and (bottom) VW+GG models.

Table 4. Percentage of Stations of ULR4 Solution in Which Stochastic Properties Are Described By Specific Colored Noise Model Component

Noise Model	Percentage of Stations
FN	71%
PL	24%
GM	2%
RW	2%
FN+RW	1%
GG	0%

uncertainties in other geodetic techniques as the two-color electromagnetic distance meter (EDM) technique [*Langbein*, 2004] and the DORIS technique [*Williams and Willis*, 2006]. Extracting a set of stations with the most optimistic uncertainties (2–3 times smaller than the PL uncertainties), we note that the estimated crossover frequency of the Gauss-Markov processes (β in equation (4)) for this set was large, with a median crossover period of 2.3 months (median crossover period was 5.5 months and 1.5 years for the whole VW+GM and VW+GG estimates, respectively). Since a higher crossover frequency represents more low-frequency spectra being uncorrelated, this estimated parameter severely affects the resulting rate uncertainty. Therefore, since the true uncertainties are unknown, we chose to be conservative and to take the stochastic model that provided the least optimistic uncertainties. Thus both Gauss-Markov models (GG and GM) were discarded as the most general noise model.

[26] Comparing velocity uncertainties derived from VW +FN and VW+PL models in Figure 3, differences were much more varied (RMS of 0.23 mm/yr), which would represent the station-by-station deviation from the fixed spectral index of the FN model. The fact that uncertainty differences were centered near zero (mean uncertainty difference is 0.02 ± 0.01 mm/yr) might indicate that, in general, the power law noise is driven by a flicker nature. In addition, the estimated mean spectral index for the VW+PL model was close to the spectral index corresponding to a flicker noise with a mean value of -0.88 ± 0.02 and a RMS of 0.27. Therefore to account properly for the mean spectral index of the time series the VW+PL model was preferred to the VW+FN. The mean noise amplitudes estimated using both VW+PL and VW+FN models were for colored noise 5.8 ± 0.1 mm $\mathrm{yr}^{-k/4}$ and 6.0 ± 0.1 mm/$\mathrm{yr}^{1/4}$, respectively, and for white noise 1.9 ± 0.1 mm and 2.0 ± 0.1 mm, respectively. The median vertical velocity uncertainty estimated using the selected noise model was 0.31 mm/yr, which represents a factor of degradation between 4 and 5 compared to that if no time correlated noise is assumed.

[27] Although the selected VW+PL model best described the GPS data used here in a general way, some stations affected by specific error sources or geophysical effects can contain a different noise type [*Langbein*, 2004]. Therefore in order to estimate the most reliable velocity uncertainty of the ULR4 vertical velocity field in a station-by-station basis, the δML value was analyzed between all the tested models. For each station, the simplest model with the highest significant ML value was selected. GM and GG noise models were however rejected if their estimated crossover frequency exceeded the semiannual frequency (about 10% of the stations). Table 4 shows a summary of the percentage of stations retained for each colored noise model component. Adopting this procedure, the main noise type of the analyzed time series is flicker noise, followed by a general power law. This way, reprocessing the GPS data with a homogeneous strategy and parameterization did not depose flicker noise as the dominant type of correlated noise content for a global GPS solution. The estimated ULR4 velocities and their correspondent uncertainties issued from the station-dependent best noise model are presented in the supplementary material. The vertical velocity uncertainties range from 0.1 to 3.3 mm/y with median value of 0.34 mm/yr.

4.4. Noise Content Time Dependency

[28] Noise analyses of global solutions are useful to get insights into the noise sources of the GPS technique. For instance, analyzing if correlated noise content is constant or time-dependent can provide relevant information about its sources. Here, we analyzed the effect of different time series lengths using synthetic and real data. In addition, we made use of real data to assess different data time period effects on estimated noise parameters.

[29] We used 54 vertical residual time series of the ULR4 solution spanning more than 12 years (1997.0–2009.0) with more than 95% of available data (minimizing possible biases resulting from data gaps). Each of these time series was windowed with a decreasing rate of 1 year, from 12 to 2 years of data (Table 5). Different periods of the same data span were analyzed separately, from the newer data (group a) to the oldest (groups b, c, d, e, or f). Table 5 summarizes the 28 different groups of time series analyzed. Each group of 54 time series corresponds to a different time series length or to a different data time period (see Table 5). Using a

Table 5. Summary of Time Series Groups Analyzed

Span/Period[a]	a	b	c	d	e	f
12	1997–2008	-	-	-	-	-
11	1998–2008	1997–2007	-	-	-	-
10	1999–2008	1997–2006	-	-	-	-
9	2000–2008	1997–2005	-	-	-	-
8	2001–2008	1997–2004	-	-	-	-
7	2002–2008	1997–2003	-	-	-	-
6	2003–2008	1997–2002	-	-	-	-
5	2004–2008	2001–2005	1997–2001	-	-	-
4	2005–2008	2001–2004	1997–2000	-	-	-
3	2006–2008	2003–2005	2000–2002	1997–1999	-	-
2	2007–2008	2005–2006	2003–2004	2001–2002	1999–2000	1997–1998

[a]The time series are distributed into 11 groups of different time series lengths (left) and in up to six groups of different data time periods (up).

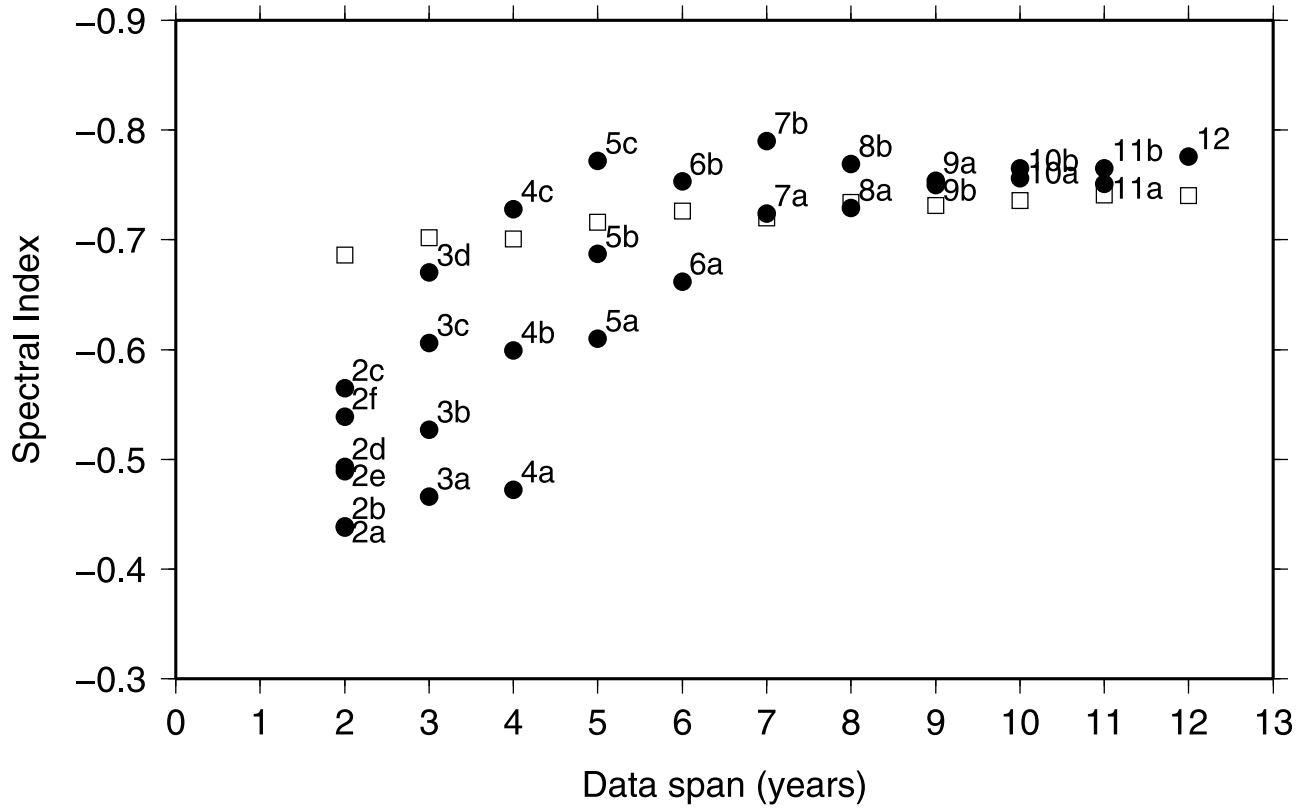

Figure 4. Median spectral index for each group of time series of Table 5 (solid circles) and for synthetic time series (open squares) with respect to time series length.

combination of PL plus WH, the median estimated noise parameters (noise amplitudes and spectral index) were extracted for each group. Estimating the trend uncertainty from short residual time series, taking into account correlated noise, causes estimated noise content to be biased low since some amount of time correlation is absorbed by the trend estimation [*Williams et al.*, 2004; *Bos et al.*, 2010]. To assess this bias on noise estimates with real data, we created 500 synthetic time series of 12 years (626 weekly points each) following the mean noise parameters of the 12-year solution. They were then windowed and analyzed as with real data.

[30] Figures 4 and 5 show the median spectral index and the median PL amplitude of each analyzed group of real and synthetic time series of Table 5. Within the synthetic data, both parameters (spectral index and colored noise amplitude) are biased slightly low for shorter time series (maximum bias of 0.1 units and 0.5 mm $yr^{-k/4}$, respectively), in agreement with the findings of *Williams et al.* [2004]. With real data, however, the spectral index and the PL amplitude of the different groups do not follow the same pattern as the synthetic data. The departure between real and synthetic data suggests that the noise content in the real time series is not constant, confirming the results of *Bos et al.* [2010]. In addition, given a time series length, incorporating older data clearly resulted in higher spectral indices (Figure 4). For example, from 3 to 8 years, spectral index of older data (b, c, or d solutions) are systematically closer to −1 than newer data (a solutions). That is, older data contain noise that is more correlated than newer data. This way, it is remarkable that with only 4 or 5 years of the oldest data (solutions 4c and 5b), the spectral index is similar to that obtained using the whole 12 years of data. Therefore noise content of long time series might be adversely affected by the noise content of the oldest data. It is worth noting that for solutions with 9 to 12 years of data, the spectral index did not change significantly by adding new and less correlated data. The spectral index started to diverge with the 8-year solutions and shorter.

[31] Regarding the amplitude of the power law noise (Figure 5), we observe the same kind of discrepancy between old and recent data analyses. In this case, the separation between older and newer data was more striking. Time series of only 2 or 3 years of the oldest data contained noise amplitude similar to that found for the whole 12 years data. In addition, solutions of 2 to 4 years using data before epoch 2001.0 (2e, 2f, 3d, and 4c solutions) were significantly noisier than other solutions of the same length. The discrepancy between older and newer solutions was also clear in the spectral index of Figure 4. In Figure 4 the discrepancies between older and newer groups start with the solutions shorter than 8 years, where the newer solution (8a) was the first one that did not use data before 2001. Therefore the year 2001 corresponds likely to a major improvement in GPS data processing.

[32] Figure 6 shows the median velocity uncertainty for each time series group of Table 5. It shows a reduction of the velocity uncertainty with time series length following a $1/T$ relationship, corresponding to a flicker noise [*Mao et al.*, 1999] (note that the noise model used was a general power law process). Regarding exclusively older (dashed

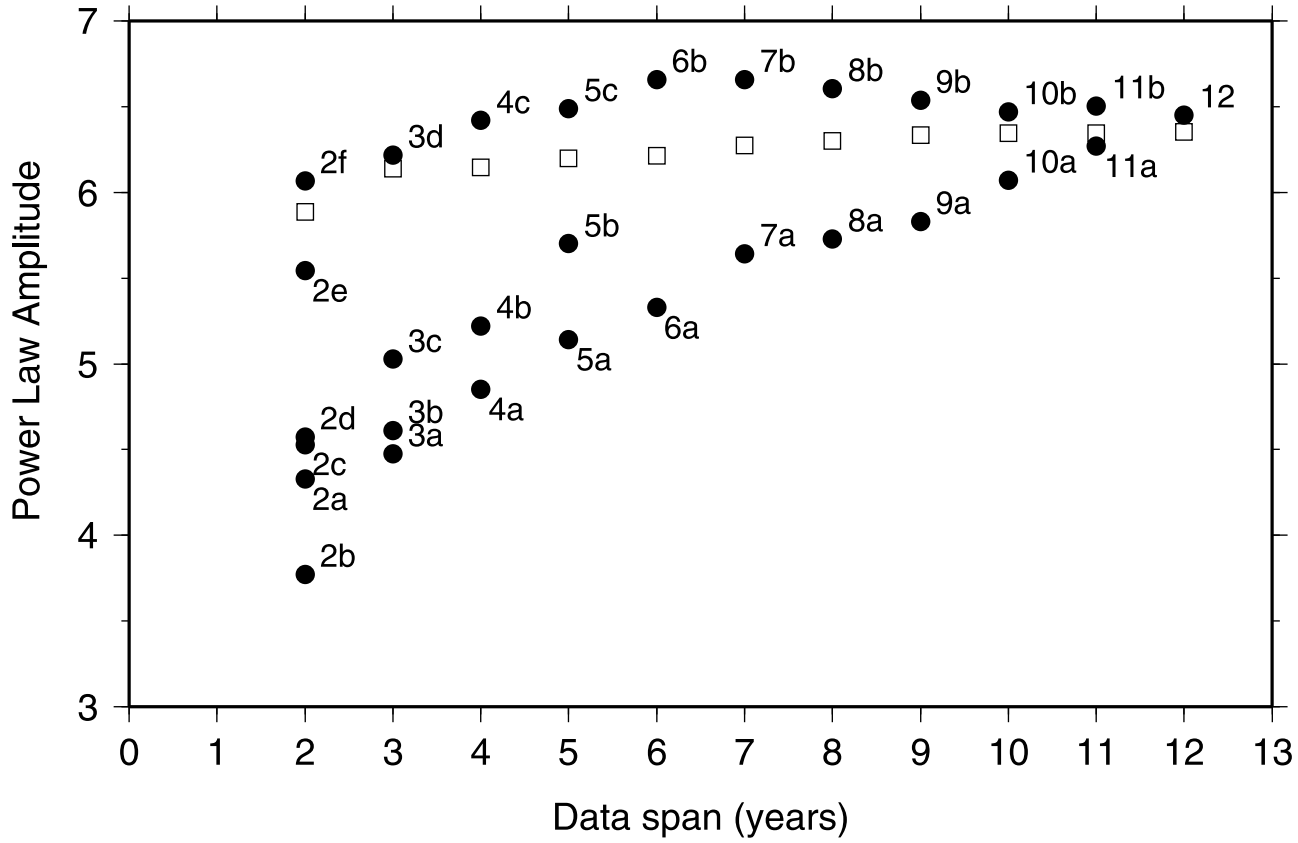

Figure 5. Median power law noise amplitude (mm $yr^{-k/4}$) for each group of time series of Table 5 (solid circles) and for synthetic time series (open squares) with respect to time series length.

line) and newer data (dotted line), the relationships between vertical velocity standard deviation and time period estimated are

$$\begin{aligned} \sigma_r^{older} &= 3.38 \cdot T^{-1.10} \\ \sigma_r^{newer} &= 1.79 \cdot T^{-0.96} \end{aligned} \quad (5)$$

being expressed in mm/yr and T in years. Equation (5) confirms that noise amplitude is significantly reduced with newer data. Figure 6 also shows the uncertainty prediction equation (25) of *Williams* [2003b] (solid line). This prediction closely matched the uncertainty estimated using older data, representing an upper bound (conservative) prediction. Equation (5) and Figure 6 show that, for instance, to reach a mean velocity uncertainty of 0.45 mm/yr, 4 years of newer data (4a) were needed against 6 years of older data (6b).

5. Discussion

[33] The discrepancy between synthetic and real data groups indicates that the correlated noise content in GPS data is not time constant. Correlated noise amplitude of the newest data (a solutions) rises linearly (Figure 5) with time series length probably because more long-period signals are being considered together with the use of noisier (older) data. Conversely, the noise amplitude of older data exhibits a convex shape (Figure 5) likely indicating that the two features (time series length and data time period) are in opposition. This way, for shorter and older time series (from 3d to 7b) noise amplitude might rise linearly with time series length. Conversely, for longer and older time series (from 7b to 12) noise amplitude might slightly decrease due to the less noisy (newer) data being added. The same noise pattern with similar amplitudes was found using the 54 selected stations from the reprocessed IGS residual vertical time series (red symbols in Figure 7) of the new ITRF2008 realization [*Altamimi et al.*, 2010]. This confirms that noise dependency on data time period is systematic for the longest time series of global GPS solutions and does not depend on our solution. For the IGS solution however, the noise separation for data before and after 2001, seen in the ULR4 solution, is less clear.

[34] In addition to this time-dependent correlated noise amplitude, *Mao et al.* [1999] found a latitudinal dependence of the white noise amplitude. *Williams et al.* [2004] also pointed out a likely latitudinal dependence of the flicker noise amplitude, being noisier in the Southern Hemisphere than in the Northern Hemisphere in both studies. Here, we analyzed 83 vertical time series (26% in Southern Hemisphere) from the ULR4 solution for which we have 95% of data between 2000 and 2009. To avoid the effect of time series length and data time period, we windowed the selected 83 time series to those epochs. For these time series, the white noise amplitude difference between Northern and Southern Hemispheres (0.18 ± 0.16 mm) was not significant. Conversely, a Student t-test showed that the Southern Hemisphere was significantly noisier with a PL amplitude difference of 1.05 ± 0.38 mm $yr^{-k/4}$. Therefore the

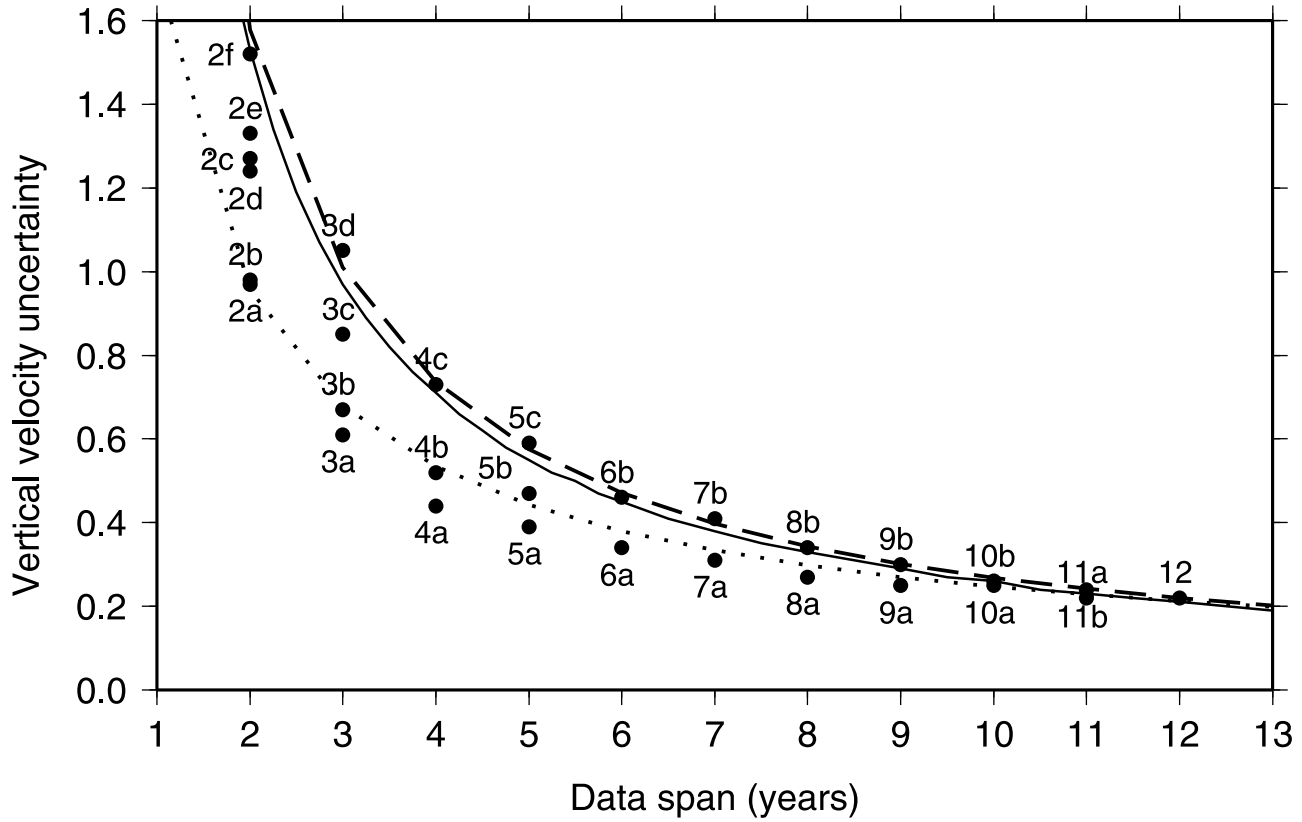

Figure 6. Median vertical velocity uncertainty (mm/yr) for each group of time series of Table 5 with respect to time series length. Fitted curves represent the relationship between data span and mean velocity uncertainty for older (dashed) and newer (dotted) data. Uncertainty prediction (solid) was estimated using equation (25) in the work of *Williams* [2003b].

correlated noise amplitude in reprocessed time series with the same length and data time period is also spatially correlated, in agreement with the findings of *Williams et al.* [2004]. The limited number of equatorial stations of our set did not allow us to confirm the parametric function used by *Williams et al.* [2004]. No difference was found on the spectral index between both hemispheres.

[35] Since spectral index and noise amplitude depend on data time period, it is clear that the noise source of this variation cannot be monument noise. This would imply an important change of the environmental conditions of all the stations had occurred, which is unrealistic. This remark supports the idea that correlated noise in current global GPS solutions is mainly related to data processing and data quality and quantity (both increasing with time) and not to monument noise. Thus even when performing a homogeneous reprocessing, the quality of the solution varies with time. Heterogeneities within the reprocessing might come from the increasing quality and quantity of stations in the tracking network, the quality and quantity of available data for each station (performance of receivers/antennas evolving with time), the evolving equipment on satellites, the quality of the orbital parameters estimation (increasing number of tracking stations with time), the tropospheric model (a priori pressure or mapping function values changing with improved ECMWF analyses) or from unmodelled differential second-order ionospheric effects (through the solar 11-year cycle) [*Petrie et al.*, 2010]. To narrow the field of possible sources down, we carried out three tests.

[36] To investigate if the noise dependency on data time period comes from the evolution in the number and density of stations in our network, the 54 stations used in the windowed noise analysis of section 4.4 were reprocessed in a unique time-constant network (see Figure 8, bottom) for the whole period (test A hereafter). These 54 stations have time series of more than 12 years with at least 95% of available data. The parameterization described in section 3 was applied. The noise analysis indicated that the correlated noise amplitude is ~34% higher corresponding with a sparser network. However, the same data time period dependency persisted (see green symbols in Figure 7), thus ruling out the tracking network evolution origin. Within this test we also estimated the orbital parameters. This way, improvements in the orbit estimation due to an increasing tracking network is also ruled out.

[37] The heterogeneity of the reprocessing of the whole network was also noticeable in the increased percentage of resolved ambiguities over time, from ~50% in 1996 (~70% in 1997) to ~95% in 2009 (not shown here, see Figure 1 of *Santamaría-Gómez et al.* [2011]). The increased percentage of fixed ambiguities in our tracking network is not related to the increased number of stations, since stations were distributed and processed in a daily variable number of subnetworks (the number of stations per subnetwork is nearly constant, between 40 and 50 from 1998 to 2009). *Tregoning*

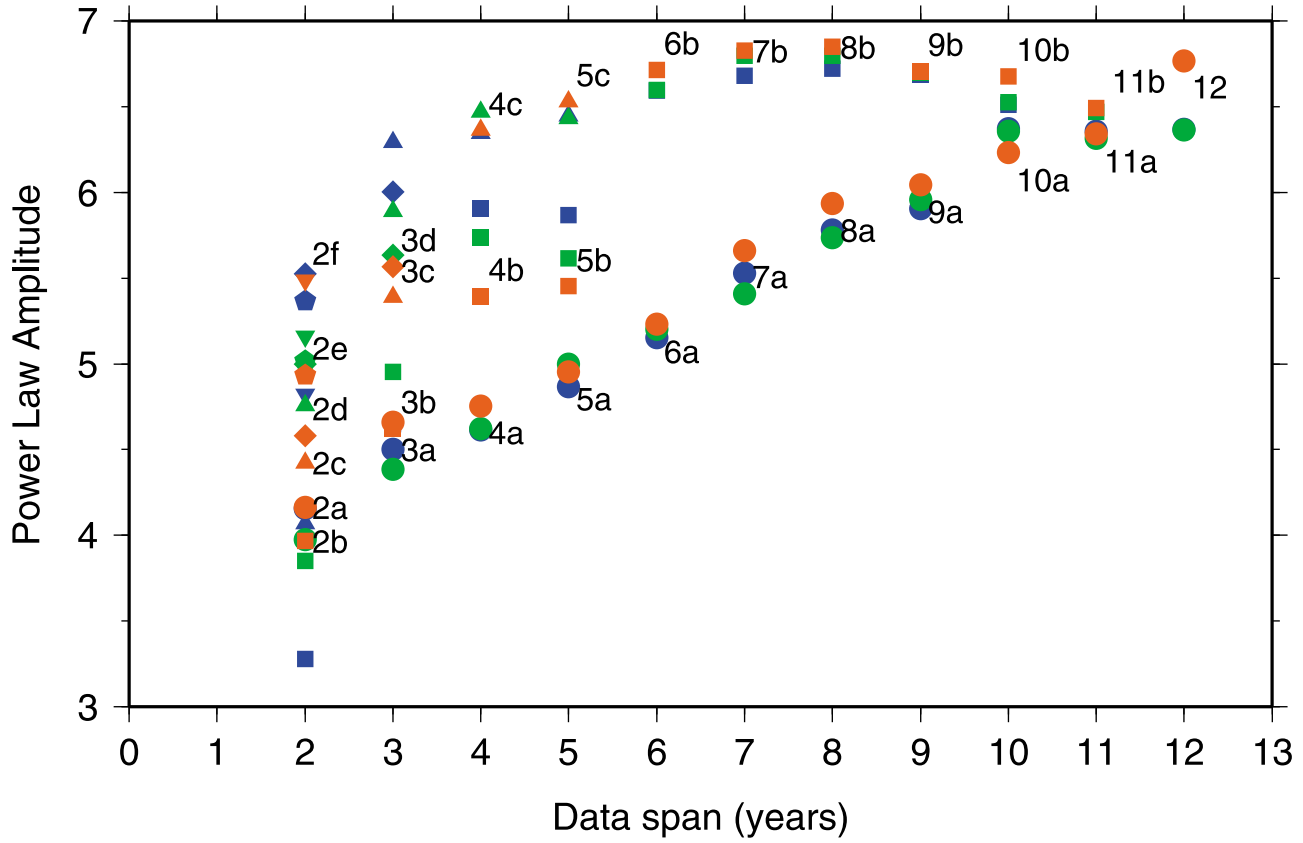

Figure 7. Median power law noise amplitude (mm $yr^{-k/4}$) for each group of time series of Table 5. Data analyzed come from the IGS/ITRF2008 solution (red) and the tests A (green) and B (blue). Each symbol represents a different data time period of Table 5, being a, circles; b, squares; c, triangles; d, diamonds; e, pentagons; and f, inverted triangles. Amplitude values correspond to the IGS/ITRF2008 solution. Amplitude values for test A and B are scaled as described in the text.

and Watson [2009] and *King and Watson* [2010] have recently shown that fixing ambiguities reduces the magnitude of power law noise and propagated spurious signals. Thus the time-evolving rate of fixed ambiguities might drive the noise dependency pattern found here. To analyze this fact, the same windowed noise analysis of the 54-station network was performed using the ambiguity-free GPS solutions (test B hereafter), i.e., no attempt to fix phase ambiguities was done. For this test, the correlated noise level was ~17% higher with respect to the ambiguity-fixed solution of test A, corroborating the findings of *Tregoning and Watson* [2009] and *King and Watson* [2010]. However, a similar pattern of data time period and time series length dependence was found again (blue symbols in Figure 7), thus rejecting the ambiguity fixation rate as the main source of this dependency.

[38] The noise pattern and the increased number of fixed ambiguities might be then related to some extent to improved receiver quality. For instance, under high ionospheric activity, the Turbo Rogue receivers (almost dominating the IGS tracking network before year 2000) had a tracking problem of L2 at low elevations (see IGS electronic mail message 2190, 1999; http://igscb.jpl.nasa.gov/pipermail/igsmail). Near the ionospheric maximum period (2001–2003), the data of a midlatitude Turbo Rogue receiver was severely affected up to an elevation of 25° (see IGS electronic mail message 2240, 1999; http://igscb.jpl.nasa.gov/pipermail/igsmail). This way, to isolate the lacking of low-elevation observations in the older data, we reprocessed the 54-station network with a cutoff angle of 30° (test C hereafter). The correlated noise amplitude of this test was ~125% higher with respect to the test A. The noise dependency (not shown in Figure 7) had a similar pattern although results were less significant due to that at least half the observations were not used (see Figure 8).

[39] The origin of the noise dependency on data time period might be then related to other causes such as quality improvements of data and models, increasing of the amount of data per station, or to the constellation evolution. In this sense, *King and Watson* [2010] showed that constellation evolution represents a clear driver for time-correlated noise content in GPS position time series. Even for a constant tracking network the number of observations (double differences) used to estimate the parameters increases with time (Figure 8). This increase might reflect the increased number of satellites and the quality improvement of the tracking equipment (number of channels, phase detection, clock noise, antenna phase stability, etc.). As receivers and antennas improve, the number and quality of the tracked phases increases, resulting both features in more observations to be inverted. This probably explains the increasing percentage of fixed ambiguities (Figure 8 on the middle) and the noise

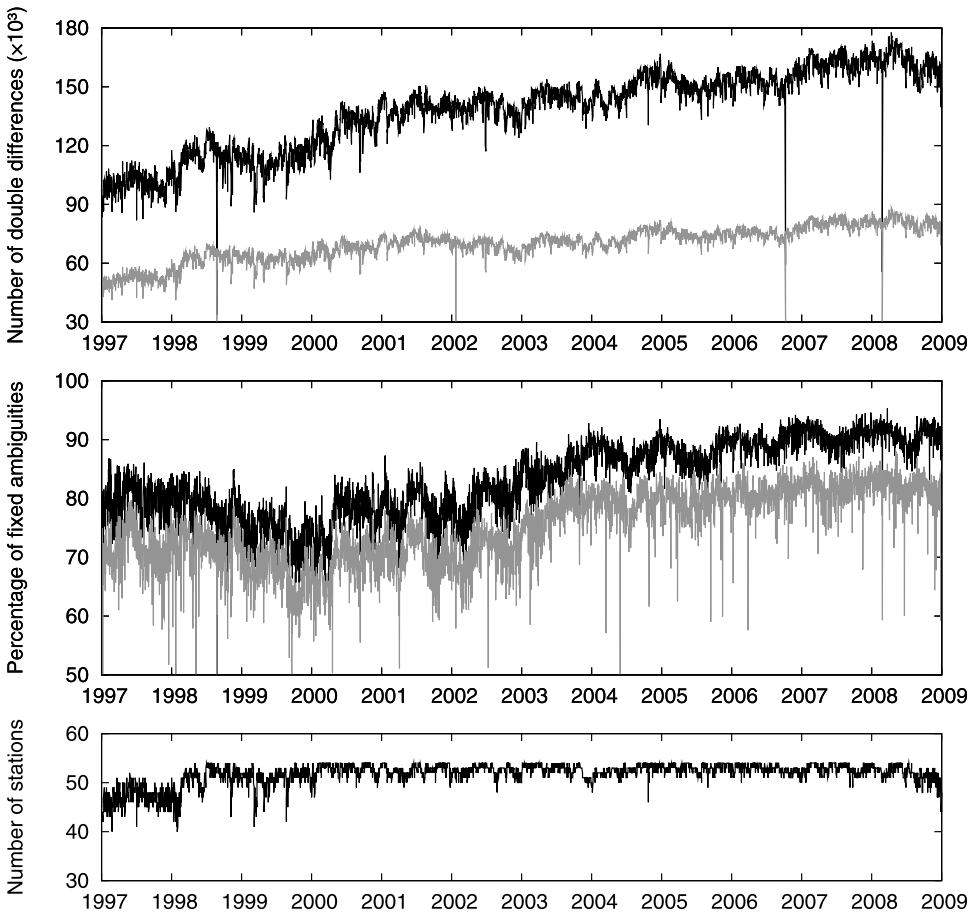

Figure 8. (top) Number of double differences, (middle) percentage of fixed ambiguities, and (bottom) number of processed stations for test A (black) and test C (gray).

pattern found here. It is worth noting that the decreasing rate of fixed ambiguities before mid 2000 in test A (Figure 8) might be related to the ionospheric effect on L2 tracking for Turbo Rogue receivers. This effect would persist even for high-elevation observations since the same phenomenon was reproduced in test C. This would indicate that even using a cutoff angle of 30° might not avoid the L2 tracking problems of older receivers under high ionospheric activity.

[40] The noise dependency on time series length and time series period would probably be larger if nonreprocessed solutions are concerned. This is illustrated by the difference of position repeatability in earlier epochs between the nonreprocessed and the most recent GPS solutions as shown in Figure 3 of *Collilieux et al.* [2010]. Thus noise content comparisons between different solutions and different regions should take into account the respective time series length and data time period included, especially within nonreprocessed solutions. For instance, *Williams et al.* [2004] compared noise content of different global and regional networks of different time series lengths (from 2 to 11 years) and different data epochs (from 1991 to 2003). *Langbein* [2008], using recent data with a median span of 6.5 years from 1996 onward, compared noise results to those of *Williams et al.* [2004] ones within the same regional network (the mean data span used by *Williams et al.* [2004] for that regional network was 3.2 years between 1991 and 2003). His results showed reduced correlated noise amplitude, in agreement with our results. *Beavan* [2005] used data from a regional network with time series lengths between 2 and 4 years from 2000 to 2004.5. He also compared his noise analysis (resulting from short and newer data) to those performed by *Williams et al.* [2004] (longer and older data) and concluded that his results were only slightly noisier. However, none of these studies took into account the fact observed here, that is, noise parameters are time-dependent.

[41] Therefore to properly account for the colored noise dependency on data time period, the known data covariance matrix used in noise analyses [e.g., *Langbein and Johnson*, 1997; *Zhang et al.*, 1997; *Mao et al.*, 1999; *Langbein*, 2004; *Williams*, 2003b; *Williams et al.*, 2004; *Amiri-Simkooei et al.*, 2007; *Bos et al.*, 2008] might take the following form:

$$C = a(t) \cdot I + b_{k(t)}(t) \cdot Q_{k(t)}(t), \tag{6}$$

where $\boldsymbol{C}$ is the data covariance matrix, $a(t)$ is the time-dependent white noise amplitude, $\boldsymbol{I}$ is the identity matrix, $b_{k(t)}(t)$ is the time-dependent colored noise amplitude of the time-dependent spectral index k, and $\boldsymbol{Q_k}$ is the noise model covariance matrix. $b_k(t)$ could be approximated, for instance, by an exponential or linear decay function. The few estimates for each time series length (maximum of 4 for 3-year solutions) did not allow however to assess the appropriateness of these functions. Note that $a(t)$ was already tested with such

an exponential decay function in the noise analysis carried out in this study (TW model, see section 4.3).

6. Conclusion

[42] We analyzed 27 noise models with 275 globally distributed stations from the ULR4 solution spanning 2.5 to 13 years to estimate their realistic vertical velocity uncertainty. Seasonal signals were previously removed when velocities were estimated. Before the noise analysis, we analyzed the remaining periodic signals in time series. Signals corresponding mainly to the GPS draconitic orbital period and its harmonics were found with amplitudes up to 4 mm. These signals might result in velocity differences up to 0.2 mm/yr, which can be neglected because estimated uncertainties (at 1 sigma) are at the same level.

[43] From the 27 noise models tested in this study, the combination of variable white noise and power law noise was the best-rated model. The power law was found to be driven mainly by a flicker noise nature (71% of the sites show flicker noise). This shows that, even within a reprocessing of more than 13 years of GPS data, flicker noise persists as the dominant colored noise for global networks. The mean noise amplitudes estimated using a power law model were 5.8 ± 0.1 mm $yr^{-k/4}$ for colored and 1.9 ± 0.1 mm for white noise. The vertical velocity uncertainty (at 1 sigma) estimated using the preferred noise model for each station ranged between 0.1 to 3.3 mm/yr with a median value of 0.34 mm/yr.

[44] We showed that correlated noise content is dependent on time series length but mainly on data time period. We found that older data are noisier than recent ones and that the same noise levels were estimated with the oldest 4–5 years and with the full 12-year time series. This fact confirms that the main noise source in global GPS solutions is not related to monuments [*King and Williams*, 2009; *Hill et al.*, 2009]. The several tests carried out in this study revealed that the increasing number of stations in the tracking network, the increasing rate of fixed ambiguities or the lack of L2 data for Turbo Rogue receivers under high ionospheric activity, are not the source of the correlated noise time-dependent pattern. Suspected sources of this time dependence are, for instance, the increasing number of data recorded per station, their improved quality, the satellite constellation evolution and the improvements of the performance of some models (i.e., tropospheric delay) used in the reprocessing.

[45] Correlated noise content comparisons between different solutions and different regions should take into account the respective time series length and data time period included, otherwise erroneous conclusions might be derived. This should be taken into account especially within non-reprocessed solutions where the time period dependence is probably larger.

[46] Using homogeneously reprocessed GPS data, our results confirmed the 1/T dependence for the velocity uncertainty first given by *Mao et al.* [1999] corresponding to a flicker noise, with T the length of the time series in years. Indeed, the vertical velocity uncertainties were estimated to decrease as ~1.8/T mm/yr with recent data against ~3.4/T mm/yr with older. For instance, to get a velocity uncertainty of 0.45 mm/yr, 4 years of recent data were needed against 6 years of older data.

[47] **Acknowledgments.** The authors acknowledge the invaluable technical support provided by Mikael Guichard, Marc-Henri Boisis-Delavaud, and Frederic Bret from the IT Center of the University of La Rochelle. The University of La Rochelle computing infrastructure was partly funded by the European Union (contract 31031–2008, European Regional Development Fund). We thank reviewers Matt A. King and Jim Ray for constructive comments which significantly improved the quality of this manuscript. Matt A. King suggested all the tests discussed in section 5. We also thank Simon D. P. Williams for helpful comments. This work was also feasible thanks to all institutions and individuals worldwide that contribute to make GPS data and products freely available (e.g., IGS, EPN, BIGF, GSI, RENAG, AMMA).

References

Agnew, D. (1992), The time domain behavior of power law noises, *Geophys. Res. Lett.*, *19*(4), 333–336, doi:10.1029/91GL02832.

Altamimi, Z., P. Sillard, and C. Boucher (2002), ITRF2000: A new release of the International Terrestrial Reference Frame for earth science applications, *J. Geophys. Res.*, *107*(B10), 2214, doi:10.1029/2001JB000561.

Altamimi, Z., X. Collilieux, J. Legrand, B. Garayt, and C. Boucher (2007), ITRF2005: A new release of the International Terrestrial Reference Frame based on time series of station positions and Earth Orientation Parameters, *J. Geophys. Res.*, *112*, B09401, doi:10.1029/2007JB004949.

Altamimi, Z., X. Collilieux, and L. Métivier (2010), ITRF2008: An improved solution of the International Terrestrial Frame, *J. Geod.* (submitted).

Amiri-Simkooei, A. R., C. C. J. M. Tiberius, and P. J. G. Teunissen (2007), Assessment of noise in GPS coordinate time series: Methodology and results, *J. Geophys. Res.*, *112*, B07413, doi:10.1029/2006JB004913.

Argus, D. F., and M. B. Heflin (1995), Plate motion and crustal deformation estimated with geodetic data from the GPS, *Geophys. Res. Lett.*, *22*(15), 1973–1976, doi:10.1029/95GL02006.

Argus, D. F., and W. R. Peltier (2010), Constraining models of postglacial rebound using space geodesy: A detailed assessment of model IGE-5G (VM2) and its relatives, *Geophys. J. Int.*, *181*, 679–723, doi:10.1111/j.1365-246X.2010.04562.x.

Argus, D. F., W. R. Peltier, and M. M. Watkins (1999), Glacial isostatic adjustment observed using very long baseline interferometry and satellite laser ranging geodesy, *J. Geophys. Res.*, *104*(B12), 29,077–29,093, doi:10.1029/1999JB000237.

Beavan, J. (2005), Noise properties of continuous GPS data from concrete pillar geodetic monuments in New Zealand and comparison with data from U.S. deep drilled braced monuments, *J. Geophys. Res.*, *110*, B08410, doi:10.1029/2005JB003642.

Bennett, R. A. (2008), Instantaneous deformation from continuous GPS: Contributions from quasi-periodic loads, *Geophys. J. Int.*, *174*, 1052–1064, doi:10.1111/j.1365-246X.2008.03846.x.

Bergeot, N., M. N. Bouin, M. Diament, B. Pelletier, M. Régnier, S. Calmant, and V. Ballu (2009), Interseismic velocity field in the central Vanuatu locked subduction zone context from GPS measurements, *J. Geophys. Res.*, *114*, B06405, doi:10.1029/2007JB005249.

Blewitt, G., and D. Lavallée (2002), Effect of annual signals on geodetic velocity, *J. Geophys. Res.*, *107*(B7), 2145, doi:10.1029/2001JB000570.

Boehm, J., B. Werl, and H. Schuh (2006), Troposphere mapping functions for GPS and very long baseline interferometry from European Centre for Medium-Range Weather Forecasts operational analysis data, *J. Geophys. Res.*, *111*, B02406, doi:10.1029/2005JB003629.

Bos, M. S., R. M. S. Fernandes, S. D. P. Williams, and L. Bastos (2008), Fast error analysis of continuous GPS observations, *J. Geod.*, *82*, 157–166, doi:10.1007/s00190-007-0165-x.

Bos, M. S., L. Bastos, and R. M. S. Fernandes (2010), The influence of seasonal signals on the estimation of the tectonic motion in short continuous GPS time-series, *J. Geodyn.*, *49*, 205–209, doi:10.1016/j.jog.2009.10.005.

Calais, E., J. Y. Han, C. DeMets, and J. M. Nocquet (2006), Deformation of the North American plate interior from a decade of continuous GPS measurements, *J. Geophys. Res.*, *111*, B06402, doi:10.1029/2005JB004253.

Cardellach, E., P. Elósegui, and J. L. Davis (2007), Global distortion of GPS networks associated with satellite antenna model errors, *J. Geophys. Res.*, *112*, B07405, doi:10.1029/2006JB004675.

Choi, K., A. Bilich, K. M. Larson, and P. Axelrad (2004), Modified sidereal filtering: Implications for high-rate GPS positioning, *Geophys. Res. Lett.*, *31*, L22608, doi:10.1029/2004GL021621.

Collilieux, X., Z. Altamimi, D. Coulot, J. Ray, and P. Sillard (2007), Comparison of very long baseline interferometry, GPS, and satellite laser ranging height residuals from ITRF2005 using spectral and correlation methods, *J. Geophys. Res.*, *112*, B12403, doi:10.1029/2007JB004933.

Collilieux, X., L. Métivier, Z. Altamimi, T. van Dam, and J. Ray (2010), Quality assessment of GPS reprocessed Terrestrial Reference Frame, *GPS Solut.*, doi:10.1007/s10291-010-0184-6.

Dong, D., T. A. Herring, and R. W. King (1998), Estimating regional deformation from a combination of space and terrestrial geodetic data, *J. Geod.*, *72*, 200–214, doi:10.1007/s001900050161.

Dow, J. M., R. E. Neilan, and C. Rizos (2009), The International GNSS Service in a changing landscape of Global Navigation Satellite Systems, *J. Geod.*, *83*, 191–198, doi:10.1007/s00190-008-0300-3.

Griffiths, J., and J. Ray (2009), On the precision and accuracy of IGS orbits, *J. Geod.*, *83*, 277–287, doi:10.1007/s00190-008-0237-6.

Gross, R. S. (2009), An improved empirical model for the effect of long-period ocean tides on polar motion, *J. Geod.*, *83*, 635–644, doi:10.1007/s00190-008-0277-y.

Herring, T. A., R. W. King, and S. C. McClusky (2008), Introduction to GAMIT/GLOBK, report, Inst. of Technol, Cambridge, Mass.

Hill, E. M., J. L. Davis, P. Elósegui, B. P. Wernicke, E. Malikowski, and N. A. Niemi (2009), Characterization of site specific GPS errors using a short-baseline network of braced monuments at Yucca Mountain, southern Nevada, *J. Geophys. Res.*, *114*, B11402, doi:10.1029/2008JB006027.

Khan, S. A., J. Wahr, E. Leuliette, T. van Dam, K. M. Larson, and O. Francis (2008), Geodetic measurements of postglacial adjustments in Greenland, *J. Geophys. Res.*, *113*, B02402, doi:10.1029/2007JB004956.

King, M. A., and C. S. Watson (2010), Long GPS coordinate time series: Multipath and geometry effects, *J. Geophys. Res.*, *115*, B04403, doi:10.1029/2009JB006543.

King, M. A., and S. D. P. Williams (2009), Apparent stability of GPS monumentation from short-baseline time series, *J. Geophys. Res.*, *114*, B10403, doi:10.1029/2009JB006319.

Kogan, M. G., and G. M. Steblov (2008), Current global plate kinematics from GPS (1995–2007) with the plate-consistent reference frame, *J. Geophys. Res.*, *113*, B04416, doi:10.1029/2007JB005353.

Kouba, J. (2007), Implementation and testing of the gridded Vienna mapping function 1(VMF1), *J. Geod.*, *82*, 193–205, doi:10.1007/s00190-007-0170-3.

Langbein, J. (2004), Noise in two-color electronic distance meter measurements revisited, *J. Geophys. Res.*, *109*, B04406, doi:10.1029/2003JB002819.

Langbein, J. (2008), Noise in GPS displacement measurements from Southern California and Southern Nevada, *J. Geophys. Res.*, *113*, B05405, doi:10.1029/2007JB005247.

Langbein, J., and H. Johnson (1997), Correlated errors in geodetic time series: Implications for time-dependent deformation, *J. Geophys. Res.*, *102*, 591–603, doi:10.1029/96JB02945.

Larson, K. M., J. Freymueller, and S. Philipsen (1997), Global plate velocities from the Global Positioning System, *J. Geophys. Res.*, *102*, 9961–9981, doi:10.1029/97JB00514.

Lyard, F., F. Lefevre, T. Letellier, and O. Francis (2006), Modelling the global ocean tides: Modern insights from FES2004, *Ocean Dyn.*, *56*, 394–415, doi:10.1007/s10236-006-0086-x.

Mao, A., C. G. A. Harrison, and T. H. Dixon (1999), Noise in GPS coordinate time series, *J. Geophys. Res.*, *104*, 2797–2816.

Marquez-Azua, B., and C. DeMets (2009), Deformation of Mexico from continuous GPS from 1993 to 2008, *Geochem. Geophys. Geosyst.*, *10*, Q02003, doi:10.1029/2008GC002278.

McCarthy, D. D., and G. Petit (2004), IERS conventions (2003), *Tech. Note 32*, 127 pp., Verl. des Bundesamts für Kartographie und Geod., Frankfurt am Main, Germany.

McClusky, S., et al. (2000), Global Positioning System constraints on plate kinematics and dynamics in the eastern Mediterranean and Caucasus, *J. Geophys. Res.*, *105*, 5695–5719.

Mignard, F. (2005), Famous, frequency analysis mapping on usual sampling, technical report, Obs. de la Cote d'Azur Cassiopée, Nice, France.

Nocquet, J.-M., E. Calais, and B. Parsons (2005), Geodetic constraints on glacial isostatic adjustment in Europe, *Geophys. Res. Lett.*, *32*, L06308, doi:10.1029/2004GL022174.

Penna, N. T., M. A. King, and M. P. Stewart (2007), GPS height time series: Short-period origins of spurious long-period signals, *J. Geophys. Res.*, *112*, B02402, doi:10.1029/2005JB004047.

Petrie, E. J., M. A. King, P. Moore, and D. A. Lavallée (2010), Higher-order ionospheric effects on the GPS reference frame and velocities, *J. Geophys. Res.*, *115*, B03417, doi:10.1029/2009JB006677.

Press, W. H., S. A. Teukolsky, W. T. Vetterling, and B. P. Flannery (1992), *Numerical Recipes in FORTRAN 77: The Art of Scientific Computing*, 2nd ed., 933 pp., Cambridge Univ. Press, New York.

Ray, J., Z. Altamimi, X. Collilieux, and T. Van Dam (2008), Anomalous harmonics in the spectra of GPS position estimates, *GPS Solut.*, *12*(1), 55–64, doi:10.1007/s10291-007-0067-7.

Santamaría-Gómez, A., M.-.N. Bouin, and G. Wöppelmann (2011), Improved GPS data analysis strategy for tide gauge benchmark monitoring, in *Proceedings of the International Association of Geodesy General Assembly, Buenos Aires, Argentina, August 31-September 4, 2009*, in press.

Schmid, R., P. Steigenberger, G. Gendt, M. Ge, and M. Rothacher (2007), Generation of a consistent absolute phase-center correction model for GPS receiver and satellite antennas, *J. Geod.*, *81*, 781–798, doi:10.1007/s00190-007-0148-y.

Schöne, T., N. Schön, and D. Thaller (2009), IGS Tide Gauge Benchmark Monitoring Pilot Project (TIGA): Scientific benefits, *J. Geod.*, *83*, 249–261, doi:10.1007/s00190-008-0269-y.

Sella, G. F., S. Stein, T. H. Dixon, M. Craymer, T. S. James, S. Mazzotti, and R. K. Dokka (2007), Observation of glacial isostatic adjustment in "stable" North America with GPS, *Geophys. Res. Lett.*, *34*, L02306, doi:10.1029/2006GL027081.

Steigenberger, P., V. Tesmer, R. Schmid, M. Rothacher, A. Rülke, M. Fritsche, and R. Dietrich (2009a), Effects of different antenna phase center models on GPS-derived reference frame, in *Geodetic Reference Frames: IAG Symposium Munich, Germany, 9–14 October 2006*, edited by H. Drewes, pp. 83–88, Springer, New York.

Steigenberger, P., M. Rothacher, M. Fritsche, A. Rülke, and R. Dietrich (2009b), Quality of reprocessed GPS satellite orbits, *J. Geod.*, *83*, 241–248, doi:10.1007/s00190-008-0228-7.

Stewart, M. P., N. T. Penna, and D. D. Lichti (2005), Investigating the propagation mechanism of unmodeled systematic errors on coordinate time series estimated using least squares, *J. Geod.*, *79*(8), 479–489, doi:10.1007/s00190-005-0478-6.

Tregoning, P., and C. Watson (2009), Atmospheric effects and spurious signals in GPS analyses, *J. Geophys. Res.*, *114*, B09403, doi:10.1029/2009JB006344.

Williams, S. D. P. (2003a), Offsets in Global Positioning System time series, *J. Geophys. Res.*, *108*(B6), 2310, doi:10.1029/2002JB002156.

Williams, S. D. P. (2003b), The effect of colored noise on the uncertainties of rates estimated from geodetic time series, *J. Geod.*, *76*, 483–494, doi:10.1007/s00190-002-0283-4.

Williams, S. D. P. (2008), CATS: GPS coordinate time series analysis software, *GPS Solut.*, *12*(2), 147–153, doi:10.1007/s10291-007-0086-4.

Williams, S. D. P., and P. Willis (2006), Error analysis of weekly station coordinates in the DORIS network, *J. Geod.*, *80*, 525–539, doi:10.1007/s00190-006-0056-6.

Williams, S. D. P., Y. Bock, P. Fang, P. Jamason, R. M. Nikolaidis, L. Prawirodirdjo, M. Miller, and D. J. Johnson (2004), Error analysis of continuous GPS position time series, *J. Geophys. Res.*, *109*, B03412, doi:10.1029/2003JB002741.

Wöppelmann, G., S. McLellan, M. N. Bouin, Z. Altamimi, and L. Daniel (2004), Current GPS data analysis at CLDG for the IGS TIGA Pilot 1Project, *Cah. Cent. Eur. Geodyn. Sismol.*, *23*, 149–154.

Wöppelmann, G., B. Martin Miguez, M. N. Bouin, and Z. Altamimi (2007), Geocentric sea-level trend estimates from GPS analyses at relevant tide gauges world-wide, *Global Planet. Change*, *57*, 396–406, doi:10.1016/j.gloplacha.2007.02.002.

Wöppelmann, G., C. Letetrel, A. Santamaría, M.-N. Bouin, X. Collilieux, Z. Altamimi, S. D. P. Williams, and B. Martín Miguez (2009), Rates of sea-level change over the past century in a geocentric reference frame, *Geophys. Res. Lett.*, *36*, L12607, doi:10.1029/2009GL038720.

Wyatt, F. (1982), Displacement of surface monuments: Horizontal motion, *J. Geophys. Res.*, *87*(B2), 979–989, doi:10.1029/JB087iB02p00979.

Wyatt, F. K. (1989), Displacement of surface monuments: Vertical motion, *J. Geophys. Res.*, *94*(B2), 1655–1664, doi:10.1029/JB094iB02p01655.

Zhang, J., Y. Bock, H. Johnson, P. Fang, S. Williams, J. Genrich, S. Wdowinski, and J. Behr (1997), Southern California Permanent GPS Geodetic Array: Error analysis of daily position estimates and site velocities, *J. Geophys. Res.*, *102*(B8), 18,035–18,055, doi:10.1029/97JB01380.

M.-N. Bouin, Centre National de Recherches Météorologiques, Météo France, 13 rue du Chatellier CS 12804, F-29228 Brest CEDEX 2, France. (Marie-Noelle.Bouin@meteo.fr)

X. Collilieux, Institut Géographique National, Cité Descartes, 6–8 Avenue Blaise Pascal, Champs-sur-Marne, F-77455 Marne-la-Vallée CEDEX 2, France. (xavier.collilieux@ign.fr)

A. Santamaría-Gómez, Instituto Geográfico Nacional, Cerro de la Palera s/n, E-19141 Yebes, Spain. (asantamaria@fomento.es)

G. Wöppelmann, Littoral Environnement et Sociétés, Université de La Rochelle, CNRS, UMR 6250, 2 rue Olympe de Gouges, F-17000 La Rochelle, France. (gwoppelm@univ-lr.fr)